**Response to review of Romain Jolivet (Referee)**

**We are grateful for the constructive feedbacks provided by Romain Jolivet. He raises three main issues, which are addressed in detail below, answering as thoroughly as possible at each point raised. Furthermore, specific comments to individual cases of the manuscript are provided. In the following, we will repeat the referee's statements and our reply to it (in bold font).**

In this article, Anderlini et al propose to apply an approach that has been applied extensively to various tectonically active regions globally but, to my knowledge, not very often to the actively deforming areas in the alps. The authors first derive some velocity fields from GNSS and InSAR data and describe some available leveling measurements. They propose a decomposition of the InSAR velocity maps into vertical and horizontal velocity fields, which are then discussed. They move on to a very classic 2D elastic modeling of the deformation to explore potential stress accumulation when considering the active faults in the region.
In general, the paper is well written and I do not see major issues with it. However, some points need to be discussed and my comments might require a bit of work. Figures are clear (although texts could be emphasized on the maps). I see three main issues in the paper that require being fixed before publication but, after that is done, this paper will be a very interesting contribution to the discussion on how active are these frontal thrusts surrounding the Alps. I hence recommend moderate revisions and I am looking forward to see a revised version of the article. I have set major revisions in the review system because there is no intermediate step between minor and major for this journal.

Main Comments:
1 - There is very little discussion on how the selection of the data is performed to avoid the effect of subsidence in the plain. The authors propose a strict threshold of -0.5 mm/yr of vertical motion below which any deformation is considered as subsidence and removed from the data fed into the model. In my opinion, this is risky, as some long wavelength subsidence might affect the general pattern of deformation. If subsidence is high near the coast and in the plain, as implied by the data, then there should be a bending effect that will affect the whole dataset. The wavelength of such bending might depend on the processes at stake, but it is unlikely that a strict threshold will allow to bypass this discussion.

**We understand the raised point. We are aware that in this region several different deformation sources are involved besides tectonic loading. Concerning the widespread subsidence in the Venetian plain, there is an extensive literature discussing all the processes involved but no bending effects are mentioned. To justify the chosen threshold, we add in Section 3.4 an in-depth description of the ongoing processes as follows: "Several studies investigated subsidence processes in the Venetian plain (e.g. Carminati and Di Donato, 1999; Carbognin et al., 2004; Teatini et al., 2005; Bock et al., 2012), which is due to three main causes (both of natural and anthropogenic non-tectonic origin): 1- aquifer compaction after the strong groundwater withdrawal in the second half of the last century (e.g. Gatto and Carbognin, 1981; Carbognin et al., 1995); 2- uncontrolled expansion of coastal settlements and industrial activities (e.g. Tosi et al., 2002); 3- recent sediment compaction (e.g. Brambati et al., 2003; Fontana et al., 2008). As we can see from the profile A-B of Fig.5, subsidence rates increase from the center of the plain towards the coasts as due to the sum of the aforementioned processes." Since none of the these processes can**

**be taken into account in our model, we choose the threshold of -0.5 mm/year and we add in the manuscript a reference to Section 3.4 to justify the choice.**

My point mainly arises from the fact that (and this is an issue) your model does not really fit the InSAR and leveling data you are using. The relatively high rates of uplift measured in the north are not correctly predicted by your model (which underdetermines uplift) while the low rates to the south are over-determined. It seems that there is a constant trend between the geodetic data and the model. Geodetic data agree well with each other, which is great, but the model does not really manage to catch up. This could also be caused by isostatic adjustment adding a long wavelength deformation (i.e. a wavelength longer than profile you have established). One possibility would be to explore the effect of a linear trend (or whatever long-wavelength pattern you can think of) that would represent the long wavelength deformation needed on top of what results from dislocations in an elastic half space. This requires exploring the tradeoff between this long wavelength deformation signal and what is predicted in terms of locking depth and slip rates for both faults. It should have an impact and should be accounted for in the inverse problem.

**As concern the uplift of the Alps, the processes responsible for this signal are: 1) active tectonic shortening, which is expected to be significant in the Eastern Southern Alps due to the active compressional Adria-Eurasia convergence 2) glacial isostatic adjustment (GIA), which is expected to be higher in the center of the Alpine chain 3) erosional unloading 4) geodynamic processes due to mantle flows. We refer to Sternai et al. (2019) for a review of the aforementioned processes. Considering that for the eastern Alps the contribution to the uplift rates due to mantle flows (process n. 4) seems to be uncertain and negligible (Sternai et al., 2019), plausible estimates of the isostatic adjustment to deglaciation (n. 2) and erosion (n. 3) may account for up to ~80% of the budget of observed uplift rates in the Eastern Alps (see Fig.8 of Sternai et al., 2019).**

**Several models have been proposed to quantify the Alpine uplift due to the glacio-isostatic contribution (e.g. Barletta et al., 2006; Spada et al. 2009; Norton and Hampel, 2010; Mey et al., 2016) and the erosional unloading (e.g. Sternai et al., 2012, 2019; Mey et al., 2016), mostly by means of large scale models with a poor spatial resolution. However, it is known that these models are less reliable at the border of the Alpine ice cap (Sternai et al., 2019), where our study area is located. In the original manuscript we widely discussed about this issue in Section 6 (L380-391), and given these uncertainties, we have not considered to correct the geodetic observations for a long-wavelength isostatic contribute. However we acknowledged its importance, stating that "a possible correction for these contributions would slightly reduce the intensity of uplift rates. If it were possible to apply such a correction, the slip-rates estimates on the fault planes could be slightly reduced, in turn decreasing a little the seismogenic potential associated with the MT and BVT faults." (L389-391).**

**In order to provide a quantitative estimate, we made a test by inverting for slip-rates and locking-depths assuming the same fault geometry, but geodetic rates corrected for a long-wavelength vertical signal, which is here assumed as a linear gradient of uplift rate along 100 km of distance. Considering the mean uplift rate of 1 mm/year in the northernmost sector of the study area (the Dolomites), we choose 0.8 mm/year (80%) as maximum vertical isostatic adjustment to be removed from the observed vertical velocities. In particular we consider a linear trend (with a slope of 0.008 mm/(year*km)) that starts from Treviso city (TREV and TVSO GPS stations), along the same direction of the profile indicated in Fig. 2, and reaching the limit of 0.8 mm/year of uplift rate in correspondence of POZZ station.**

**We are aware that this model is purely speculative and based on strong assumptions, but we can consider this simple approach as an upper-bound case on how considering or not these long-wavelength signal may affect the results of the inversion.**

**We remove this linear signal from all the geodetic datasets, i.e. from the vertical component of GPS velocities, leveling data and subsampled InSAR LoS rates, and perform the inversion of the modified velocities in order to estimate locking depths and slip rates for the proposed fault geometry. Due to these changes in the input observations, we re-evaluate the relative weighting factor *Wsar*, finding an optimal value of 0.68.**

**The results of the inversion are presented in the Figure A1 (below), showing the same information reported in Figure 7 of the manuscript with a few differences: the purple line in the section of the vertical rates represents the linear gradient we removed, and light gray dots indicate the unmodified original datasets, while all the other data are corrected for the linear gradient. In the bottom panel the estimated parameters (locking depth and dip-slip rates) are reported, as well as in the following table.**

| Dataset | LD Montello Ramp | LD Bassano Ramp | Slip rate Montello Ramp | Slip rate Montello Flat | Slip rate Bassano Ramp | Slip rate Deep Ramp | RMSE GPS | RMSE LEV | RMSE InSAR |
|---|---|---|---|---|---|---|---|---|---|
| Corrected data | 4.6 km | 8.6 km | 0.5 mm/a | 0.35 mm/a | 2.0 mm/a | 2.3 mm/a | 0.46 mm/a | 0.57 mm/a | 0.59 mm/a |
| Original Data | $5.6_{-3.8}^{+3.5}$ km | $9.1_{-0.6}^{+1.3}$ km | $0.5_{-0.1}^{+0.2}$ mm/a | 0.4 ± 0.1 mm/a | $2.1_{-0.6}^{+0.8}$ mm/a | $2.5_{-0.7}^{+0.8}$ mm/a | 0.44 mm/a | 0.72 mm/a | 0.66 mm/a |

**We observe that there are no substantial differences with respect to the optimal fault parameters obtained with the original dataset (Table 2 of manuscript, also reported above). This correction lead to a slight decrease of slip rates and locking depths, which are, however, all largely within the error bounds of the optimal model. We can note that at the expense of a slight increase of GPS RMSE, the misfit for the other data decreases, allowing for a better balancing among the three dataset. The slight increase of GPS residuals is mainly due to the misfit between the model and the vertical velocities to the north (see PASS and FDOS in the figure below) that depends, however, on the vertical gradient we remove which is steeper than the gradients expected from large scale models. In light of these results we do not aim at correcting the geodetic velocities for an isostatic uplift signal, considering also that the estimated fault parameters doesn't provide significant differences in terms of slip-rates and locking depths. Most of these considerations have been added in Section 6 of the main text and the specific details in the Supplement.**

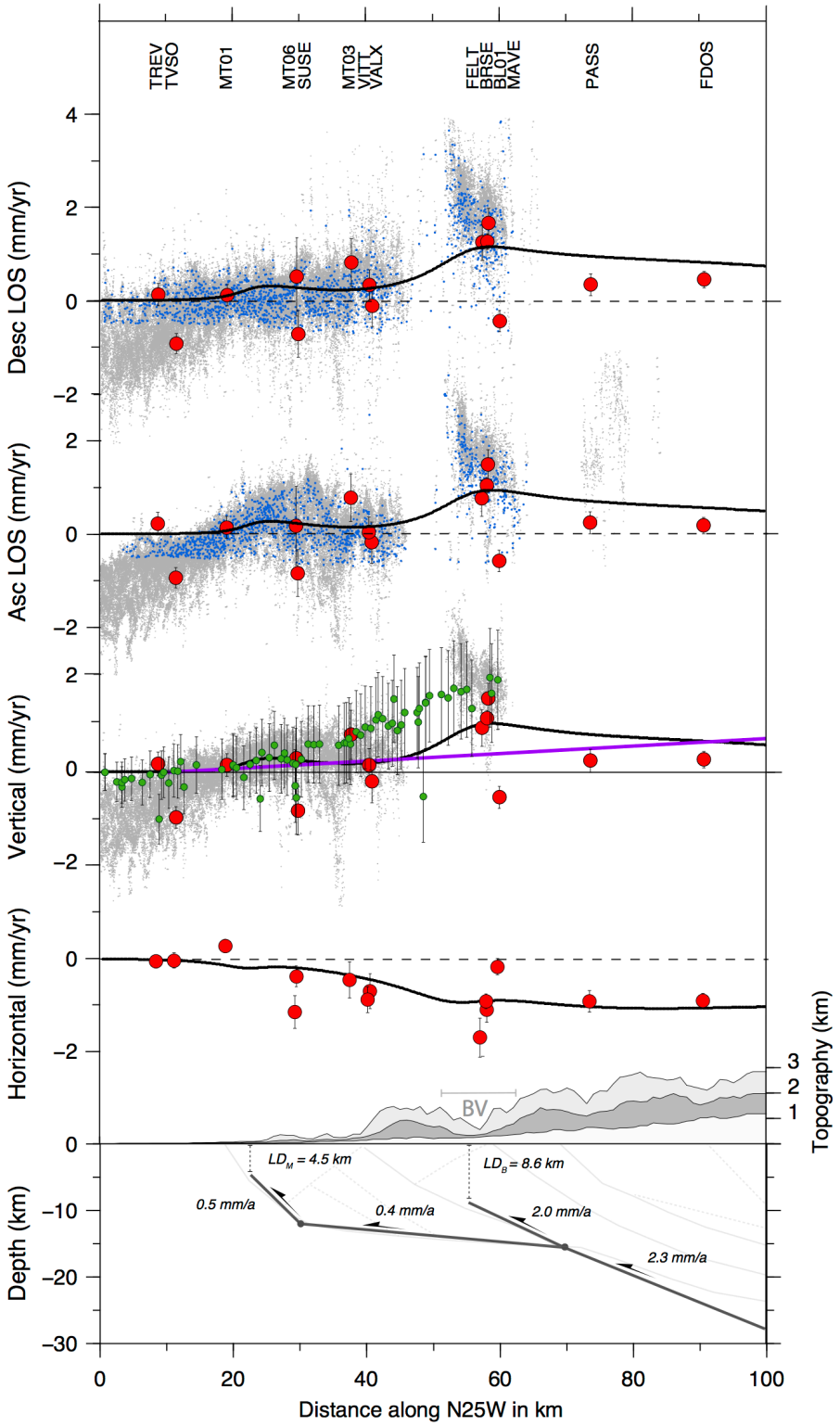


**Figure A1: Cross sections, across the A-B profile of Fig. 2 of the manuscript, showing the modeled (black lines) horizontal and vertical velocities, as well as the SAR ascending and descending LoS rates, along with the measured ones. Green points indicate leveling data and small blue dots represent the subsampled InSAR LOS rates used during the inversion. The bottom panel reports the optimal fault geometry with dip-slip rates and locking depths estimates. BV: Belluno valley**

2 - There is not enough details on how the InSAR data have been processed. Although the SBAS method is now quite known, quantitative information is required to assess the quality of the velocity field. It is not only because it correlates quite well with GPS that everything has been done right. For instance, correcting for tropospheric delays using a phase-topography correlation when trying to unravel a signal that correlates as well with topography is dangerous. One could easily mix deformation with tropospheric delays.

**We used the SARScape module of ENVI software, provided by Harris Geospatial Solutions (http://sarmap.ch/tutorials/sbas_tutorial_V_2_0.pdf), to perform SBAS analysis. The SBAS algorithm includes several steps (e.g Pasquali et al. 2014): creation of a connection graph (computing all differential interferograms from the input image stack according to the chosen criteria for temporal and geometric baselines), differential interferogram generation (spectral shift and adaptive filtering), phase unwrapping, orbit refinement and re-flattening, first estimation of the average displacement, atmospheric phase screen removal, and final estimation of the average displacement and mean ground velocity. In our study, we achieved a ground resolution of 90 m by using a multi-looking factor of 4 in range and 20 in the azimuth. All the Single Look Complex images (SLC) are coregistered in the master image geometry using a 90-m Digital Elevation Model (DEM) provided by the Shuttle Radar Topography Mission (SRTM). The topographic phase contribution was removed using the DEM, too. We applied the Goldstein filter (Goldstein and Werner, 1998) to smooth the differential phase and use precise DORIS orbits (provided by the European Space Agency) and the SRTM DEM to correct the computed interferograms from possible orbital ramps. We used the Delauney minimum cost flow (MCF) network (Constantini, 1998) along with the Delaunay method to unwrap the differential interferograms. The unwrapping coherence threshold at this stage was set to 0.3. We selected approximately several tens Ground Control Points (GCP) mainly at the borders of the processed frame, to perform the refinement and re-flattening step. Subsequently, the average displacement rate and residual height-correction factors were estimated by inverting a linear system through the Singular Value Decomposition method. Then, low-pass and high-pass spatial filters were used for the time-series images, to screen and remove the atmospheric phase component. In fact, the starting idea is that atmosphere is correlated in space but not in time. We considered two moving windows of 365 days and 1200 meters for the two filters (High and low pass). Finally, the solution of the inversion was geocoded through the used DEM. All of the final displacement measurements were obtained onto the satellite line of sight (LOS) direction and geocoded in the UTM 33N reference system.**

Furthermore, since the region has quite strong topographic gradients, unwrapping is probably challenging and there is not a word on that (which method is used for unwrapping? In general, which software is used to compute the interferograms?).

**As mentioned above, we adopted the Minimum Cost Flow (MCF) algorithm with the Delauney triangulation method. The latter helps the propagation of the unwrapping solution to reach coherent pixels also if they are separated by non-coherent areas. In fact, as you can see from in Figure 4 of the main text, the solution was able to overcome only the first mountainous chain propagating through the valleys. This was exactly due the presence of quite strong topographic gradients, as the reviewer has noticed. All the A-InSAR processing chain, as already mentioned above, was computed using the Sarscape software.**

Would it be possible to see a baseline plot?

**Yes, the following figure shows the obtained connections graph and baselines distribution for the ASAR-Envisat datasets of both ascending and descending orbits. We choose interferometric pairs with a perpendicular baseline smaller than 450 meters and a temporal baseline lower than 600 days for both the orbits. The figure is now added in the Supplement.**

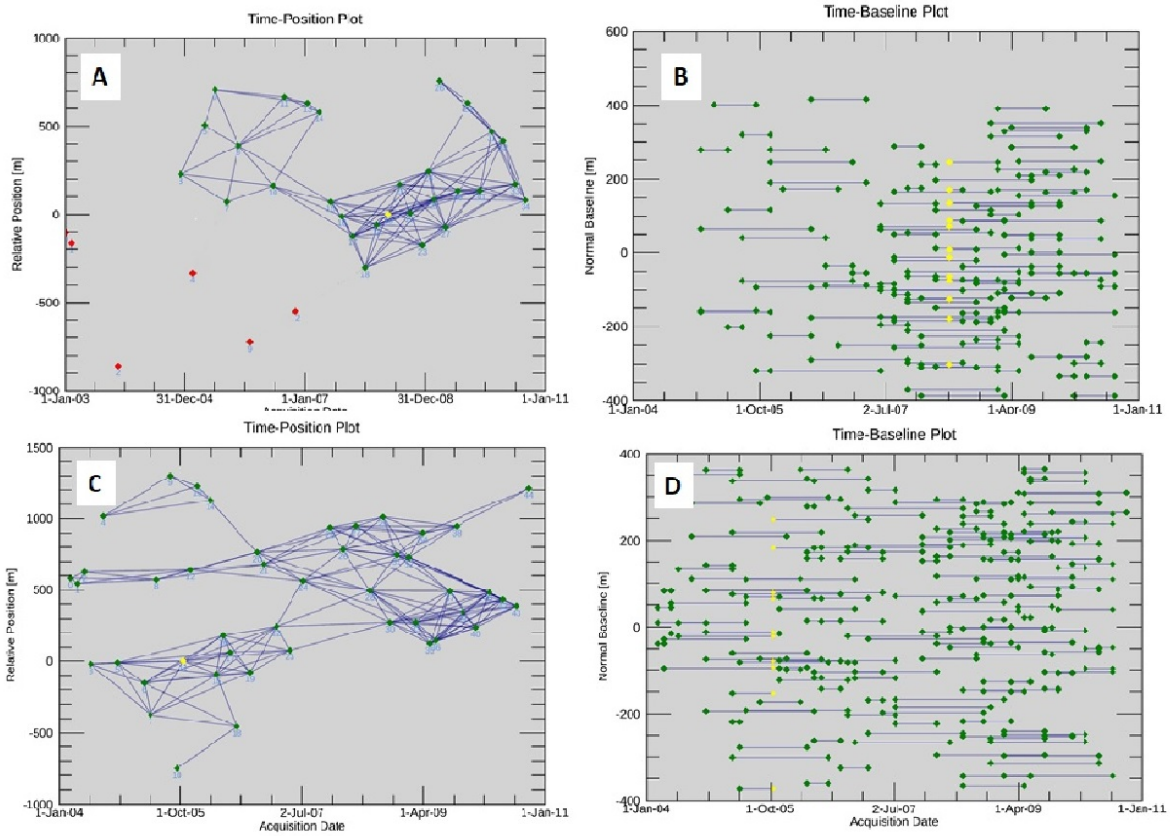


**Fig. A2: (A) Considered pairs connection graph for the descending SAR orbit; (B) Considered baseline graph for the descending SAR orbit; (C) Considered connection graph for the ascending SAR orbit; (D) Considered baseline graph for the ascending SAR orbit.**

Also, is there connectivity issues within the network, considering potential unwrapping issues?

**Looking at Figure A2, we are confident that no remarkable unwrapping issues were found during such a step. Moreover, before following the inversion steps, we checked each interferogram discarding all the pairs showing clear unwrapping errors and keeping the ones with low atmospheric noise.**

What is the RMS of the reconstruction of your time series?

**We calculate the RMS considering one of the different possible formulas and exactly the following:** $RMSError = \sqrt{1 - r^2} SD_y$ **where *SDy* is the standard deviation of each retrieved displacement time series and *r* is the correlation coefficient between the time series and the considered acquisitions. RMS is a measure of the fitting quality geocoded. It is the RMSE expressed in millimeters. The higher this value the worse the fitting and inversion quality. The RMS about all the time series retrieval is showed in the figure A3:**

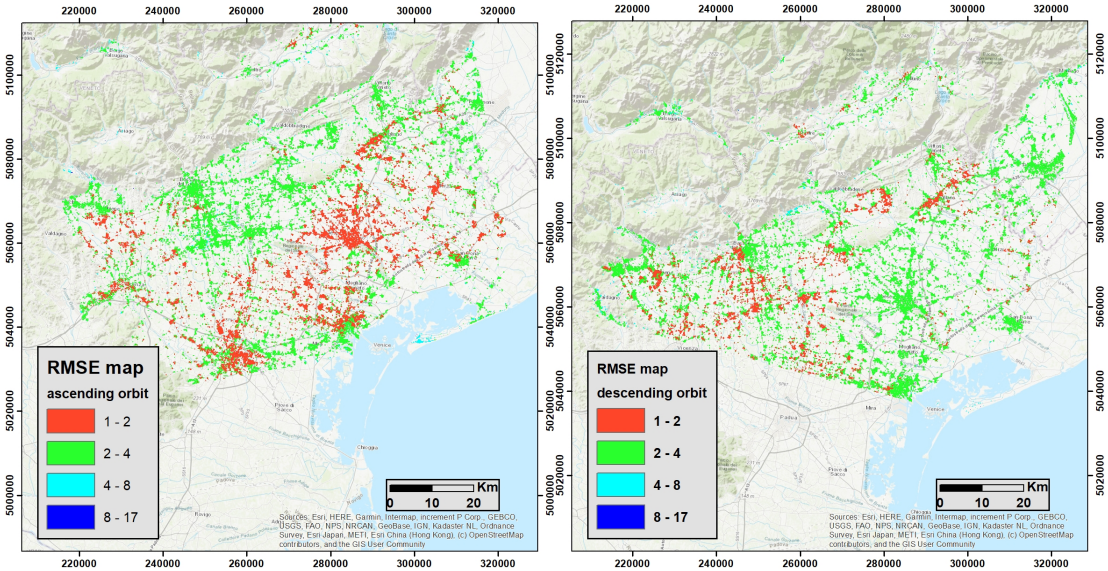


**Fig. A3: RMSE maps of the displacement time series for the ascending and descending orbits**

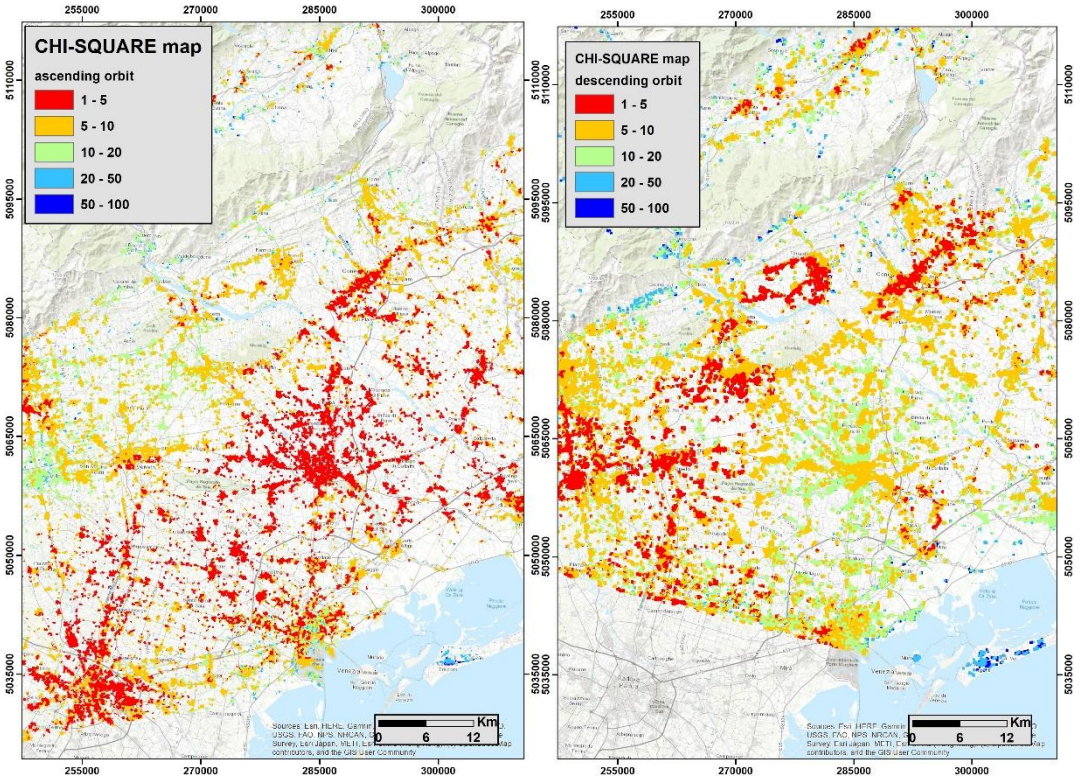


**Fig. A4: Chi-Square values for the ascending and descending orbits**

How linear is the time series?

**Initially, we considered a linear model in the inversion step then, in a second unwrapping run, the non-linearity is estimated from the residuals obtained as difference from the unwrapped phase and the linear model. One of the estimated parameters at the end of the processing chain is the Chi-square value (Figure A4) relative to each time series. Such a value is a non-dimensional number representing how much the time series diverges from the linear behavior. Low values of the Chi-square indicates a quasi-linear trend of the displacement time series, high values for the contrary. In any case, the Chi-square test has**

**to be considered carefully. In fact, high values do not mean not reliable result for that area. In fact the chi-square does not represent an absolute but relative parameter, in the meaning that it does not have a predefined maximum value (i.e. the interferometric coherence parameter) but can vary depending on the type of the movement present in the study area. So if there are zones with a non-linear behavior, such areas will show high chi-square values and vice-versa. In our case, high values of chi-square are greater than 100, thus values within 10-15% of the maximum can be considered representative of pixels having mostly linear behavior.**

Is there a time dependent signal?

**The retrieved patterns are mainly time independent, in the meaning that the most of the obtained ground deformation field shows a behavior tending towards the linear trend (red and orange areas in Figure A4)**

There is much more details provided for the processing of GPS data and the processing of InSAR being much less standardized than GPS these days (especially with the old Envisat data) suggests there is a lot to be added in the manuscript.

**We added much more info about the processing steps and the parameters setting adopted during the processing chain in the manuscript and in the Supplement.**

Finally, a lot of people have developed comparable methods for InSAR downsampling and they deserve some credit (see Lohman & Simons 2005, Jolivet et al 2012, 2015 or Sudhaus & Jonsonn 2009 for instance, but there is many other papers mentioning this).

**We agree with the reviewer, there is a lot of literature regarding downsampling methods of InSAR data and we add now a short description in Section 4: "Most of literature regarding downsampling methods of InSAR data analyzes coseismic and volcanic ground deformation. In these cases just a portion of the displacement map is characterized by high deformation gradient, thus the widely-used quadtree sampling method (e.g. Jónsson et al., 2002; Pedersen et al., 2003; Lohman and Simons, 2005; Metzger et al., 2011; Barnhart and Lohman, 2013) is appropriate. Indeed this algorithm reduce the number of data in order to represent the statistically significant portion of the signal (Jónsson et al., 2002) choosing a specific threshold value for the data variance in each iteration. This method has been applied also for interseismic studies (e.g. Jolivet et al., 2012; Maurer and Johnson, 2014; Xue et al., 2015) where, however, the signal-to-noise ratio of InSAR data is big enough to define an appropriate threshold value to avoid losing information of the deformation gradients. In our case, with low deformation gradients it is highly risky to apply a subsampling method that depends on the deformation signal itself. For this reason we apply an alternative method that uniformly reduce the density of pixels and the specific technical details are provided in the Supplement."**

3 - The description of the inversion procedure is incomplete. The algorithm used to find the minimum of the cost function should be, at least, named.

**We integrate the main text in Section 4 as follows: "The inversion method exploits a constrained, non-linear, derivative-based optimization algorithm (i.e. interior-point, see Byrd et al., 1999; Waltz et al., 2006). It allows to estimate the optimal parameter solution corresponding to a possible global minimum of the cost function representing the misfit between the model prediction and the geodetic measurements. These algorithms depend on the gradient and higher-order derivatives in order to guide them through misfit space, thus they can get trapped in a local minimum (Cervelli et al., 2001), providing the best results when the starting point is near the global minimum. However, in order to ensure that we find a global solution in the inversion, we tested several different initial guess founding always the same model estimate."**

Furthermore, I suspect there is some regularization of the inverse problem involved (maybe not), but please mention it.

**No, there is no regularization of the inverse problem, but we applied specific constraints to the parameter space to be investigated (such as locking depth within the elastic thickness and slip rates kinematically consistent among them). Indeed, we did not modify the relationship of the cost function (as it would be done in case of a regularization) that considers only the weighted misfit between observed and modeled velocities, but we took advantage of the specific options of the minimization algorithm described above, forcing the model to respect the imposed constraints.**

In addition, the data covariance is not described. How is it determined? One cannot follow the deal with weights if one cannot reconstruct the covariance matrix.

**We add in the manuscript in Section 4 the description of the data covariance: "The data covariance matrix is computed as follows:** $cov = \Sigma R \Sigma^T$ **where** $\Sigma$ **is the diagonal matrix of data uncertainty and *R* is the data correlation matrix, that is dimensionless, equal to one along the diagonal and the off-diagonal elements representing the correlation between each couple of data. Assuming the three geodetic dataset (GPS, InSAR and leveling) independent among them, the whole covariance matrix is composed by three independent blocks, one for each dataset. The correlation values are nonzero only for the three components of each GPS site, considering the measurements obtained by the GPS stations to be uncorrelated among them, and for the leveling data, following the approach of Árnadóttir et al. (1992). The InSAR data covariance matrix is instead diagonal with equal variance of 1 mm$^2$/year$^2$ for all the pixels."**

Then, there is a problem in the a posteriori covariance discussion. The authors mention the a posteriori covariance is derived for the linear terms while bootstrap is used for the non-linear terms. In my opinion, the covariance that is derived here is obtained considering the least squares criterion (without regularization? with regularization? Is it just GˆT Cdˆ{-1} G ?) but then, it only corresponds to a "slice" of the model space, that slice corresponding to the best non-linear parameters obtained. If so, the a posteriori covariance is greatly underestimated as it is only representative of a joint marginal of the full a posteriori PDF.

**We estimated the a-posteriori covariance matrix considering the least squares criterion (without regularization), but we agree with the reviewer that this is a partial representation of the slip rate uncertainties. We consider now to use the bootstrap distributions both for the linear and non-linear model terms providing the errors at 95% confidence bounds. Please see the answer below and the further specific details of the adopted approach. The error bounds for the estimated parameters have been corrected in Table 2 and in Figure 7 of the manuscript. For a full description of the model parameters uncertainties we provide also the trade-off distributions between parameters pairs, replacing Figure S6 of the supplementary material with the Figure A5 shown below. We can observe from these distributions that the locking depth estimates do not show any correlation with the other parameters, while for the dip-slip rates the strict correlation among them is representative of the kinematic conservation constraint, for which the only parameter we can consider independent is the deep decollement slip rate (underlined label of Figure A5). We have modified accordingly the main text, discussing in Section 5 the results in terms of fault parameters error bounds from the frequency histograms and of possible correlation between parameters from the trade-off scatter plots.**

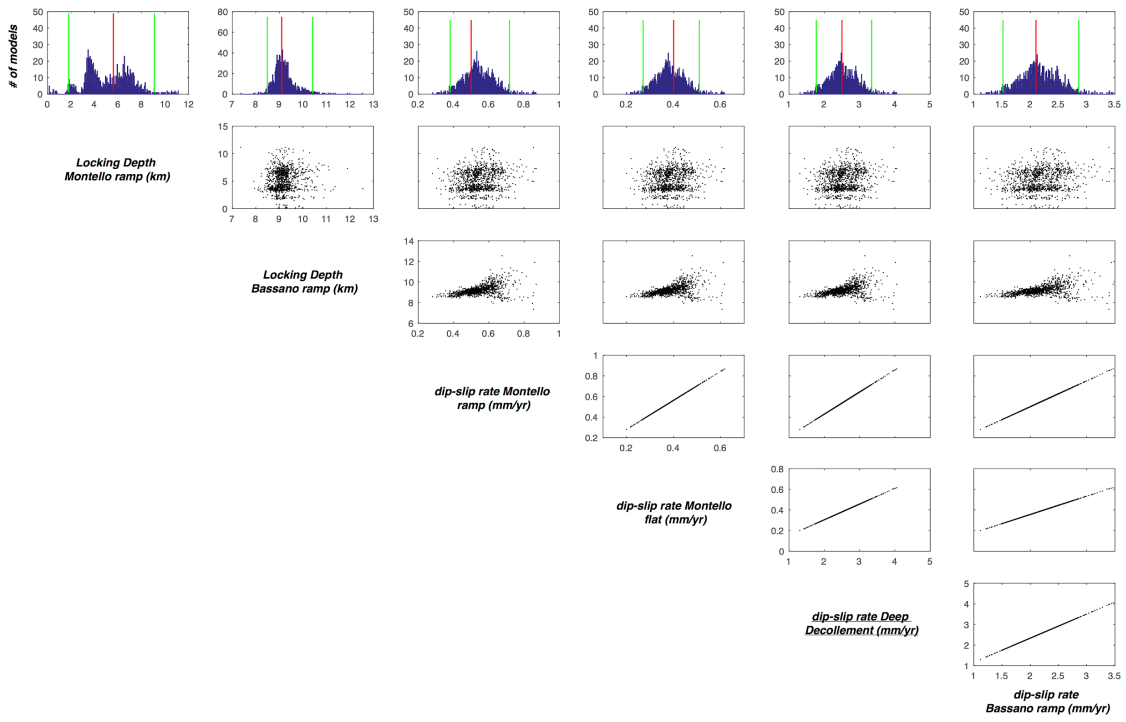


**Fig A5: Model parameters distribution, obtained from the inversion of 1000 bootstrap re-samples of the original data (see Section 5). Top row: frequency histograms of the optimal fault parameters with the best optimal model (red line) and boundary values of 95 percentile confidence interval (green lines); see Table 2 for specific values. Other rows: scatter plots showing trade-off between parameter pairs.**

Finally, one can see in supplementary material figure S6 that the range of possible models for the locking on the Montello Ramp is bi-modal.

**Figure S6 (now, top row of Figure A5) doesn't show the range of possible models, but the collection of the optimal models we obtain randomly resampling the data by means of a bootstrap procedure used to estimate confidence intervals of the derived parameters (Segall and Davis, 1997) without making assumptions about the underlying statistics of**

**errors (Amoruso and Crescentini, 2008). This method reflects the limitation of the data set used (Cervelli et al., 2001), and the bi-modal behavior of the locking depth of the Montello Ramp should be interpreted as representative of the low capability of the data to constrain this parameter, for which indeed the deformation signal is close to the techniques limits and velocity measurements appears noisy. These considerations are now added to the manuscript in Section 5 to provide a more complete description of the error bounds definition.**

Then, if it is not Gaussian, why choosing the mean model?

**We didn't choose the mean model but the optimal model estimated by the inversion algorithm, described above, using the whole geodetic dataset.**

It seems that some models could be more appropriate. Would it be possible to sample for all the possible models using a Monte Carlo approach, which would give all the tradeoffs between the various parameters (and potentially solve the issue raised in my first comment)?

**The bootstrap resampling provides optimal model distribution and the tradeoffs between the various parameters as shown in Figure A5.**

For the minor comments, please refer to the annotated pdf I have sent along with my review.

**We corrected the minor comments annotated in the pdf.**

Looking forward to read an improved manuscript, if I am required to do so. I also strongly encourage the authors to add their geodetic data (i.e. the GPS, InSAR and leveling rates presented in the paper) to an online repository so other scientists can have a go at the modeling, once this study is published.

**Since the GPS and leveling rates are already available in the Supplement, only InSAR velocities are made available in an online repository.**

Please also note the supplement to this comment:
https://www.solid-earth-discuss.net/se-2020-10/se-2020-10-RC2-supplement.pdf

**References**

**Amoruso, A., Crescentini, L., 2008. Inversion of synthetic geodetic data for the 1997 Colfiorito events: clues on the effects of layering, assessment of model parameter PDFs, and model selection criteria. Ann. Geophys., 51, doi:10.4401/ag-3027.**

**Árnadóttir, T., Segall, P., and Matthews, M., 1992. Resolving the discrepancy between geodetic and seismic fault models for the 1989 Loma Prieta, California, earthquake, Bulletin of the Seismological Society of America, 82, 2248–2255.**

**Barletta, V. R., C. Ferrari, G. Diolaiuti, T. Carnielli, R. Sabadini, C. Smiraglia, 2006. Glacier shrinkage and modeled uplift of the Alps, Geophys. Res. Lett., 33, L14307, doi:10.1029/2006GL026490**

**Barnhart, W. D., R. B. Lohman, 2013. Vertical partitioning of strain during earthquake sequences in Iran: Phantom earthquakes and triggered aseismic creep, Geophys. Res. Lett., 40, 819–823, doi:10.1002/grl.50201.**

**Bock, Y., S. Wdowinski, A. Ferretti, F. Novali, A. Fumagalli, 2012. Recent subsidence of the Venice Lagoon from continuous GPS and interferometric synthetic aperture radar, Geochem. Geophys. Geosyst., 13, Q03023, doi:10.1029/2011GC003976.**

**Brambati, A., L. Carbognin, T. Quaia, P. Teatini, L. Tosi, 2003. The Lagoon of Venice: Geological Setting, Evolution and Land Subsidence, Episodes, 26, 264-268.**

**Byrd, R.H., Hribar, M. E., Nocedal, J. 1999, "An Interior Point Algorithm for Large-Scale Nonlinear Programming," SIAM Journal on Optimization, Vol 9, No. 4, pp. 877–900.**

**Carbognin L., L. Tosi, P. Teatini, 1995. Analysis of actual land subsidence in Venice and its hinterland (Italy). In: Barends J.F., et al. (1995, eds.) - Land Subsidence, 129-137, A. A. Balkema, Rotterdam**

**Carbognin, L., P. Teatini, L. Tosi, 2004. Eustacy and land subsidence in the Venice Lagoon at the beginning of the new millennium. J. Marine System, 51(1–4), 345– 353.**

**Carminati, E., G. Di Donato, 1999. Separating natural and anthropogenic vertical movements in fast subsiding areas: The Po plain (N. Italy) case, Geophys. Res. Lett., 26, 2291–2294, doi:10.1029/1999GL900518.**

**Costantini, M. 1998. A novel phase unwrapping method based on network programming. IEEE Trans. Geosci. Remote Sens., 36, 3, 813-821, DOI: 10.1109/36.673674**

**Fontana, A., Mozzi, P., Bondesan, A., 2008. Alluvial megafans in the Veneto-Friuli Plain: Evidence of aggrading and erosive phases during Late Pleistocene and Holocene. Quaternary International, 189(1), 71–90**

**Gatto, P., Carbognin, L., 1981. The Lagoon of Venice: Natural environmental trend and man-induced modification. Hydrological Science Bulletin, 26(4), 379– 391**

**Goldstein, R., Werner, C., 1998. Radar interferogram filtering for geophysical applications. Geophysical Research Letter, 25, 21, 4035-4038, DOI: 10.1029/1998GL900033.**

**Jolivet, R., C. Lasserre, M.-P. Doin, S. Guillaso, G. Peltzer, R. Dailu, J. Sun, Z.-K. Shen, and X. Xu, 2012. Shallow creep on the Haiyuan Fault (Gansu, China) revealed by SAR Interferometry, J. Geophys. Res., 117, B06401, doi:10.1029/2011JB008732**

**Jònsson, S., H. A. Zebker, P. Segall, F. Amelung, 2002. Fault slip distribution of the 1999 Mw7.1 Hector Mine, California, earthquake, estimated from satellite radar and GPS measurements, Bull. Seismol. Soc. Am., 92(4), 1377–1389, doi:10.1785/0120000922.**

**Lohman, R. B., M. Simons, 2005. Some thoughts on the use of InSAR data to constrain models of surface deformation: Noise structure and data downsampling, Geochem. Geophys. Geosyst., 6, doi:10.1029/2004GC000841**

**Maurer, J., K. Johnson, 2014. Fault coupling and potential for earthquakes on the creeping section of the central San Andreas Fault, J. Geophys. Res. Solid Earth, 119, doi:10.1002/2013JB010741.**

**Metzger, S., Jónsson, S., Geirsson, H., 2011. Locking depth and slip-rate of the Húsavík Flatey fault, North Iceland, derived from continuous GPS data 2006–2010. Geophysical Journal International, 187: 564-576. doi:10.1111/j.1365-246X.2011.05176.x**

**Mey, J., Scherler, D., Wickert, A.D., Egholm, D.L., Tesauro, M., Schildgen, T., Strecker, M.R., 2016. Glacial isostatic uplift of the European Alps. Nature Commun. https://doi.org/10.1038/ncomms13382.**

**Norton, K.P., Hampel, A., 2010. Postglacial rebound promotes glacial re-advances – a case study from the European Alps. Terra Nova 22 (4), 297–302.**

**Pasquali, P., Cantone, A., Riccardi, P., Defilippi, M., Ogushi, F., Gagliano, S., Tamura, M., 2014. Mapping of ground deformations with interferometric stacking techniques, Land Application of Radar Remote Sensing, Holecz, F., Pasquali, P., Milisavljevic, N., Closson, D., IntechOpen, DOI: 10.5772/58225. Available online**

**Pedersen, R., Jònsson, S., Àrnadòttir, T., Sigmundsson, F. Feigl, K.L., 2003. Fault slip distribution of two June 2000 Mw6.5 earthquakes in South Iceland estimated from joint inversion of InSAR and GPS measurements, Earth. planet. Sci. Lett., 213(3–4), 487–502. doi:10.1016/S0012-821X(03)00302-9.**

**Segall, P., Davis, J. L., 1997. GPS applications for geodynamics and earthquake studies, Annu. Rev. Earth Planet. Sci., 23, 201–336.**

**Spada, G., Stocchi, P., Colleoni, F., 2009. Glacio–isostatic adjustment in the po plain and in the northern adriatic region. Pure Appl. Geophys. 1303–1318. https://doi.org/10.1007/s00024-004-0498-9.**

**Sternai, P., Herman, F., Champagnac, J.-D., Fox, M., Salcher, B., Willett, S.D., 2012. Preglacial topography of the European Alps. Geology 40 (12), 1067–1070.**

**Sternai, P., Sue, C., Husson, L., Serpelloni, E., Becker, T.W., Willett, S.D., Faccenna, C., Di Giulio, A., Spada, G., Jolivet, L., Valla, P., 2019. Present-day uplift of the European Alps: evaluating mechanisms and models of their relative contributions. Earth-Sci. Rev., 190, 589-604. https://doi.org/10.1016/j.earscirev.2019.01.005**

**Tosi, L., Carbognin, L., Teatini, P., Strozzi, T., Wegmüller, U., 2002. Evidence of the present relative land stability of Venice, Italy, from land, sea, and space observations, Geophysical Research Letters, 29(12), 1562, doi:10.1029/2001GL013211.**

**Waltz, R. A. , J. L. Morales, J. Nocedal, and D. Orban, 2006. "An interior algorithm for nonlinear optimization that combines line search and trust region steps," Mathematical Programming, Vol 107, No. 3, pp. 391–408.**

**Xue, L., S. Schwartz, Z. Liu, L. Feng, 2015. Interseismic megathrust coupling beneath the Nicoya Peninsula, Costa Rica, from the joint inversion of InSAR and GPS data, J. Geophys. Res. Solid Earth, 120, 3707–3722, doi:10.1002/2014JB011844.**